Characterization of a CCD-camera-based system for measurement of the solar radial energy distribution

To cite this article: A Gambardella and R Galleano 2011 *Meas. Sci. Technol.* **22** 105902

Meas. Sci. Technol. **22** (2011) 105902 (9pp) doi:10.1088/0957-0233/22/10/105902

Characterization of a CCD-camera-based system for measurement of the solar radial energy distribution

A Gambardella and R Galleano

European Commission, Joint Research Centre, Renewable Energy Unit, TP 450, I-21027 Ispra (VA), Italy

E-mail: attilio.gambardella@jrc.ec.europa.eu

Received 13 April 2011, in final form 28 June 2011
Published 2 September 2011
Online at stacks.iop.org/MST/22/105902

Abstract

Charge-coupled device (CCD)-camera-based measurement systems offer the possibility to gather information on the solar radial energy distribution (sunshape). Sunshape measurements are very useful in designing high concentration photovoltaic systems and heliostats as they collect light only within a narrow field of view, the dimension of which has to be defined in the context of several different system design parameters. However, in this regard the CCD camera response needs to be adequately characterized. In this paper, uncertainty components for optical and other CCD-specific sources have been evaluated using indoor test procedures. We have considered CCD linearity and background noise, blooming, lens aberration, exposure time linearity and quantization error. Uncertainty calculation showed that a 0.94% ($k = 2$) combined expanded uncertainty on the solar radial energy distribution can be assumed.

Keywords: charge-coupled device (CCD), linearity, blooming, solar radial energy distribution (sunshape)

(Some figures in this article are in colour only in the electronic version)

1. Introduction

Charge-coupled device (CCD) cameras are widely used in many fields of science and technology as a powerful tool for carrying out certain types of measurements (e.g. reflectance or transmittance evaluation of inhomogeneous objects or assessment of source uniformity) that would otherwise be performed by means of scanning devices, and, in general, for obtaining information from complex scenes [1–4]. Meteorology, solar photometry and concentrating photovoltaics (CPV) are more recent and promising application fields [5, 6].

This extensive range of applications is a result of their high resolution, high quantum efficiency, wide spectral response, low noise, linearity (which simplifies the handling of pixel values), fast response, small size, low power consumption and durability. In addition, since a CCD is based on multiple sensing elements of equal size, the device provides precise spatial quantization allowing accurate spatial representation of images in a computer [7]. However, since CCD detectors are two-dimensional devices (unlike photodiodes), they present additional challenges for response characterization due to charge transfer and other electronics-related problems.

The solar radial energy distribution (also referred to as 'sunshape') can be measured by a high resolution CCD scientific camera-based system, according to the rationale proposed in [5]. The advantage of such a system is that the required tracking accuracy is low, the alignment is simple and, under specific conditions, it is linear over four orders of magnitude. Sunshape data at different locations are very useful in designing/characterizing high concentration CPV because these systems collect light only within a narrow field of view (FOV) containing the solar disk and a small portion of the circumsolar region [8, 9]: for instance, a CPV system with a concentration ratio of around 500× typically has a FOV of less than 3° [10, 11]. Pyrheliometers, which are routinely used to measure direct solar beam irradiance, typically have a FOV of 5° to 6° and give no information on the radial energy distribution of the incident solar light within their FOV. Because pyrheliometer measurements include a

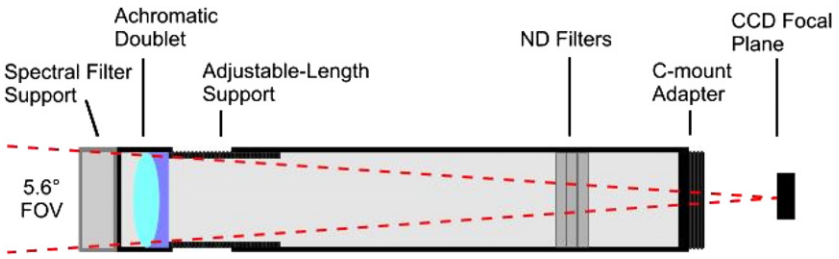

Figure 1. A scheme of the setup with the custom-made optics.

large portion of the circumsolar radiation, depending on the concentration ratio, they can overestimate the amount of direct sunlight that would be collected by a CPV system. Moreover, the lack of information about radial energy profiles, which influences flux and radiant energy distribution on the focal plane of a CPV system, makes the pyrheliometer less useful when designing/characterizing such a system. The added value provided by the CCD camera is the capability to obtain a multi-pixel image with high spatial resolution which allows inferring information on the solar radial energy distribution within its FOV. Hence, it is possible to separate and analyze contributions from the solar disk and the sun-aureole under the hypothesis/constraint that the sum of the irradiances associated with the CCD pixels, relevant to the 5°–6° solid angle, is the same as that of the pyrheliometer.

This paper describes the setup for sunshape measurements, the analysis of the main uncertainty sources, together with the characterization of the system response linearity. Provided the system is working within its linearity range, an absolute irradiance calibration is not needed for sunshape analysis; pyrheliometer data are used to scale measurements performed at different irradiance levels.

2. Measurement setup

The measurement system employs a camera with a back-illuminated CCD array with 512 × 512 pixels, each pixel having a size of 24 × 24 μm^2. This camera delivers a 16-bit digital signal (65 536 gray levels). The CCD signal is digitized inside the camera head and the chip is thermoelectrically cooled to −70 °C to reduce thermal noise and stabilize the background noise. Furthermore, the camera has a mechanical shutter which prevents the chip from being illuminated during pixel readout, thus avoiding smearing effects.

The entrance optics consists of a 125 mm (25 mm ∅) fixed focal achromatic doublet lens. The achromatic doublet uses BK7 and SF5 lenses to allow wavelength transmission from visible (VIS) to near infrared (NIR). The lens system was designed to have a FOV of about 5.6°. The above-mentioned FOV, coupled with the 512 × 512 pixel CCD array, results in a system angular resolution of 0.011°. The custom-made optics has been designed with a 5.6° FOV to ensure that, also in the case of pointing/tracking errors, the irradiance coming from a cone pointed at the sun and 5° wide (i.e. the FOV of the pyrheliometer considered in this study) is measured by the CCD camera. A set of neutral density filters, to reduce incoming sunlight, and a set of seven band-pass optical filters, to explore the energy contents in different spectral regions within camera spectral response, complete the setup (see figure 1).

Table 1. Main characteristics of the measurement system.

Digital CCD camera	
Manufacturer and model	Andor Ikon M912BV
Digitalization	16-bit
No of sensor elements	512 × 512 pixels
Pixel size	24 × 24 μm^2
Spectral response	300–1100 nm
Optics	
Lens	Achromatic doublet
Substrate	N-BK7/N-SF5
Coating	VIS–NIR
Focal length	125 mm (fixed)
Diameter	25 mm
FOV	5.6°
Angular resolution	0.01°

The measurement system is mounted on a two-axis solar tracker having a pointing accuracy better than 0.1° in both elevation and azimuth. The main characteristics of the system are listed in table 1.

3. Measurement system response characterization and budget uncertainty

Indoor tests were performed in order to estimate the accuracy of the measurement system and characterize its response. In all of the experiments except one, an integrating sphere is used to obtain a spatially distributed Lambertian light source. The illumination source is a continuous wave halogen lamp; integrating sphere and exit port diameters are 6 and 1 inches, respectively. The uncertainty of the integrating sphere spatial uniformity is less than 1%.

Preliminary tests let us identify the following parameters as the best compromise configuration: counts background corrected as data type, single scan acquisition mode, image readout mode, 50 Hz at 16-bit as the readout rate, and no pre-amplification. The main uncertainty sources considered for characterizing the measurement system response were background noise, pixel linearity, blooming, lens aberration and exposure time linearity. The following budget uncertainty has been evaluated according to [12] and all considered components have been treated as non-correlated.

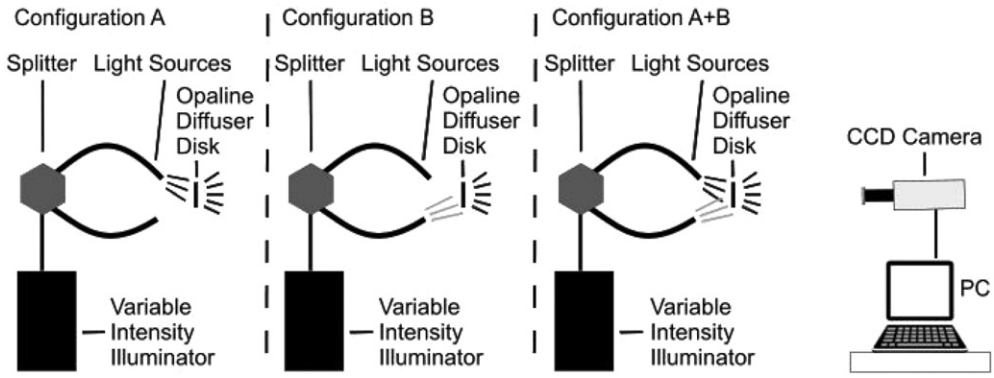

Figure 2. Scheme of the first experimental setup to evaluate linearity of the camera system.

3.1. Background noise

Background noise is related to the dark current signal. The dark current is produced by thermally excited electrons. The expected number of excited electrons is proportional to the integration time and is temperature dependent. Cooling reduces the dark current.

The CCD-camera operating software easily allows measurement of background noise. Hence, once the CCD was cooled to −70 °C the system acquired several raw background data (i.e. data in uncorrected counts, acquired in the darkness). Successively, the background noise, measured over 40 acquisitions, was statistically analyzed (average and standard deviation values (counts) are 908 and 7, respectively) and its average value has been considered to correct the sunshape image (e.g. background corrected image).

The measured average CCD noise level was found to be less than 1.38% of the system dynamics (16-bit) with a standard deviation of less than 0.01%. Therefore, background noise corrected images have a residual standard uncertainty of 0.01% ($k = 1$).

3.2. Pixel linearity

The working hypothesis is that, provided the measurement system is operating within its linearity range, an absolute pixel irradiance calibration is not needed and pyrheliometer data can be used to scale measurements taken at different irradiance levels. To evaluate pixel linearity, two indoor experiments have been carried out. In both cases a linearity test, as described in [13], has been performed on the experimental results. As a reference, when the standard deviation divided by the slope of the linear fit is below 0.02 it means that the hypothesis of linearity holds with an uncertainty of at maximum 2%. Above this value, for our needs, the linearity is not acceptable.

In the first experiment the system measured an opaline diffusive disk simulating the solar disk. The disk is illuminated by two light sources (fiber optic bundles) first switched on alternatively (configurations A and B) and then simultaneously (configuration A+B). The light sources are fed by a variable intensity illuminator set at different intensity levels in order to test the linearity in the entire camera dynamic range. Figure 2 shows the first experimental setup. During the experiment, the light intensity is increased until the A+B measurement saturates (visually detected by blooming on the acquired images), as it is well known that when pixels are saturated the linearity hypothesis no longer holds. The detailed analysis of blooming is shown in the next sub-section.

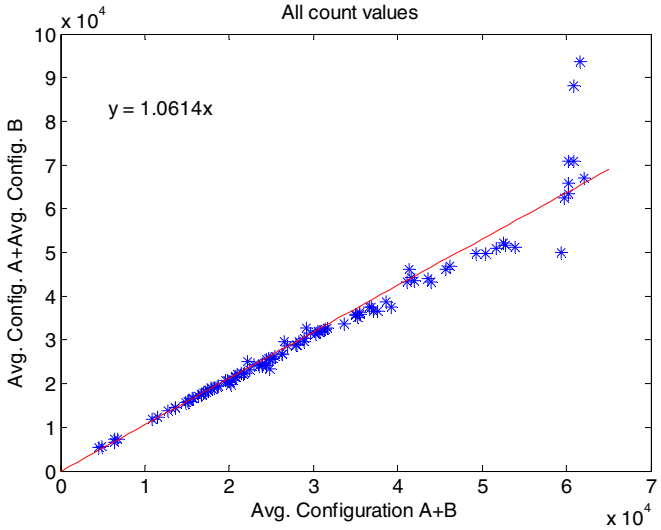

Figure 3. Configuration A+B average values plotted against the corresponding configuration A plus configuration B ones.

The rationale behind the experiment is that under the hypothesis of linearity the mathematical sum of the brightness of the two light sources measured separately should match that measured when both light sources are on.

Average values corresponding to the brightness of the disk radiating surface (expressed in counts) for different intensities of the source lights were evaluated for the three aforementioned configurations. Successively, average values of configuration A+B are plotted against the corresponding configuration A plus configuration B ones (see figure 3). For reference purposes this plot also shows the linear fitting (the solid line) and its equation (top-left part). The visual quality of the fit is confirmed by the correlation coefficient (0.9682) and the linearity test (1.18%).

It is also noted that close to the pixel saturation value, the graph shows some outliers. The same analysis has been performed excluding pixel count values greater than 56 000, corresponding to a dynamic range greater than 15.7 bits. This guarantees a cut-off below the saturation point. The results are

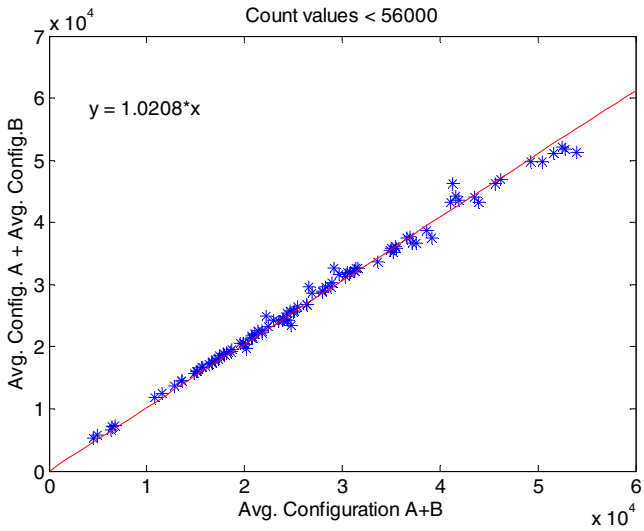

Figure 4. Configuration A+B average values, which are below the value of 56 000, plotted against the corresponding configuration A plus configuration B ones.

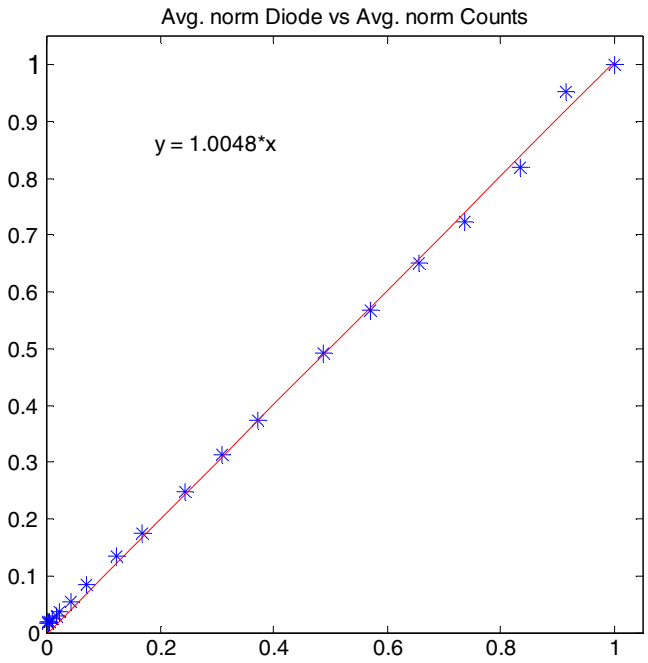

Figure 6. Average normalized photodiode values plotted against the corresponding measures of the CCD camera.

shown in figure 4 and show a correlation coefficient of 0.9975 and linearity within 0.35%.

The second experiment involves an integrating sphere simulating the solar disk, the measurement system and a photodiode. The experimental setup is shown in figure 5.

The rationale behind this is as follows: by using a photodiode with a linear response [14] the comparison of the photodiode output signals and the system measurements at increasing luminance intensity levels provides a linearity test showing the ranges in which the camera system has a linear response. As in the previous case, the light intensity is increased up to the level at which the measurements saturate.

Before performing the linearity test a pre-elaboration on both photodiode and system measurement outputs was made to make the data comparable. The photodiode outputs were normalized to their maximum value. System measurement sub-images, corresponding to the exit port of the integrating sphere, were first averaged one by one and then normalized to the highest intensity sub-image. Subsequently, normalized values from the photodiode and the system measurements were plotted against each other (see figure 6) and the linearity test performed.

The clear linear relationship is confirmed by the correlation coefficient (0.9985) and the linearity test results (0.67%). During this test the measured brightness of the radiating surface ranged from 906 (i.e. background noise level) to 58 745 counts (dynamic range greater than 15.8 bits). As in the previous case, the same analysis has been performed excluding counts greater than 56 000, giving as result a correlation coefficient of 0.9984 and linearity within 0.33%.

Before proceeding further, it must be noted that, since we always considered average values of the whole exit port of the integrating sphere, the uncertainty due to the source spatial non-uniformity can be considered included in these uncertainty results.

In conclusion, a pixel linearity response with a dynamic range greater than 15.7 bits was experimentally verified. Therefore, if the system measurements are kept below the

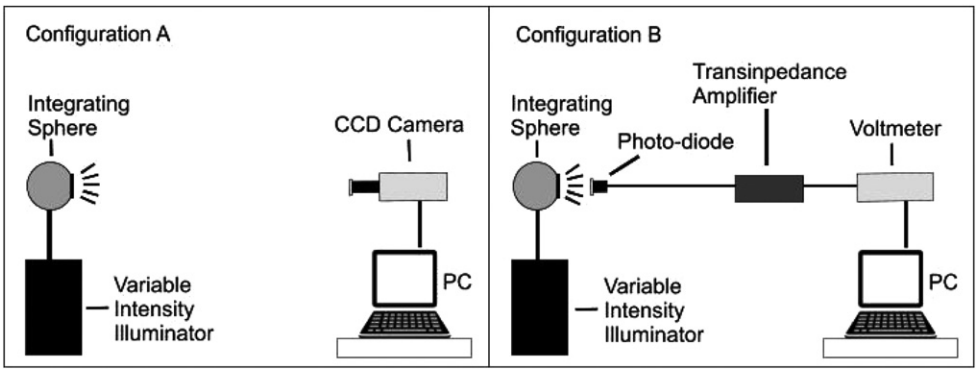

Figure 5. The second experimental setup to evaluate linearity of the camera system.

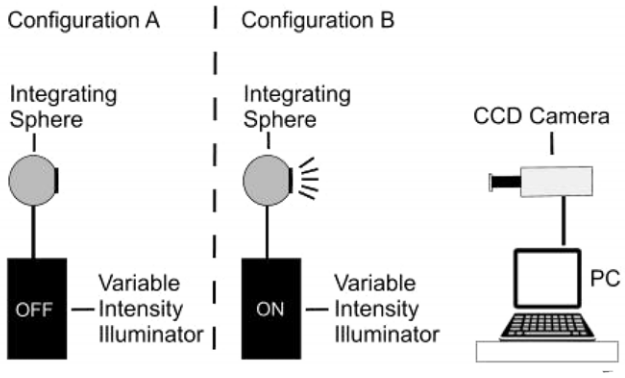

Figure 7. The experimental setup to evaluate residual blooming.

56 000 count value, a standard uncertainty component due to pixel nonlinearity of 0.35% ($k = 1$) can be assumed.

3.3. Blooming

One of the most important issues in the response characterization of a CCD-based measurement system is the assumption that pixels respond independently. When this assumption is violated the stored charge in a pixel overflows from one potential well and mixes with the charge in the neighboring pixel's potential well. This effect is known as blooming. If blooming is present the relationship between the output counts and the irradiance is nonlinear [1].

Even below saturation blooming may be present and can cause smearing on the acquired image in the spatial region corresponding to the transition between the solar disk and the sun-aureole, which is the one we are interested in. Moreover, the finite spatial resolution of the camera system has to be taken into account. To evaluate this, area measurements of the exit port of an integrating sphere under two different conditions (illuminated and not illuminated, see figure 7) were performed and compared.

The hypothesis behind this experiment is that the evaluation of the area mismatch of the images of the radiating surface in the two configurations can give an estimation of the residual blooming effect. Figure 8 shows images corresponding to the two configurations. The same squared area (110 × 110 pixels) has been considered and the pixel values have been normalized to their corresponding maximum values, which were equal to 6850 counts for configuration A and 61 370 counts for configuration B, i.e. slightly above the considered linearity threshold. Edge detection has been performed to highlight and compute the area of the radiating surfaces (see figure 9). The difference in areas is below 0.04%

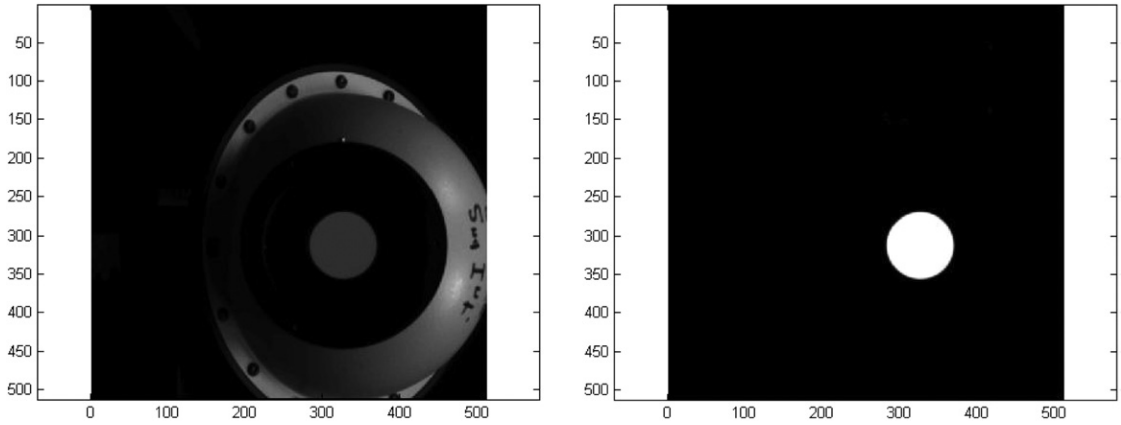

Figure 8. Images of the CCD camera acquisition with the integrating sphere off (left) and on (right).

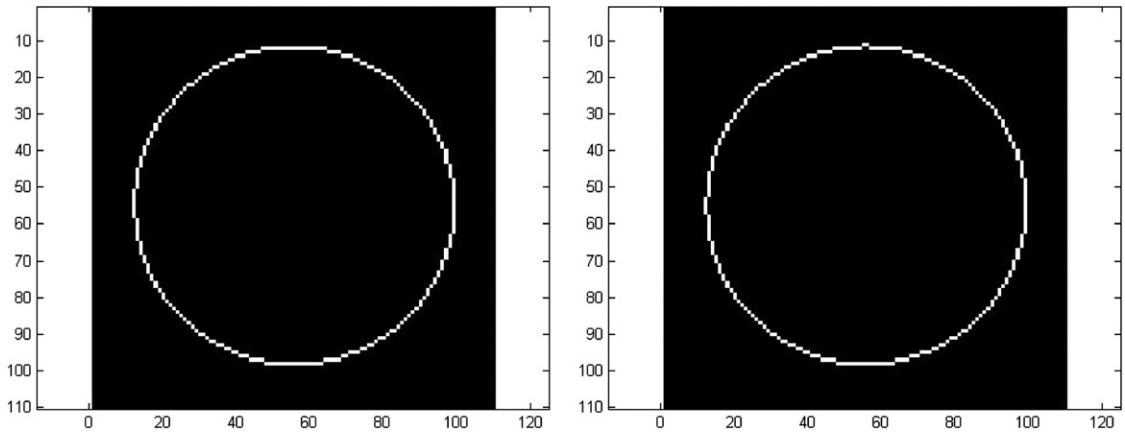

Figure 9. Edge detection has been performed to highlight the area of the radiating surface; the left image is with the integrating sphere switched off and the right one is for the integrating sphere switched on.

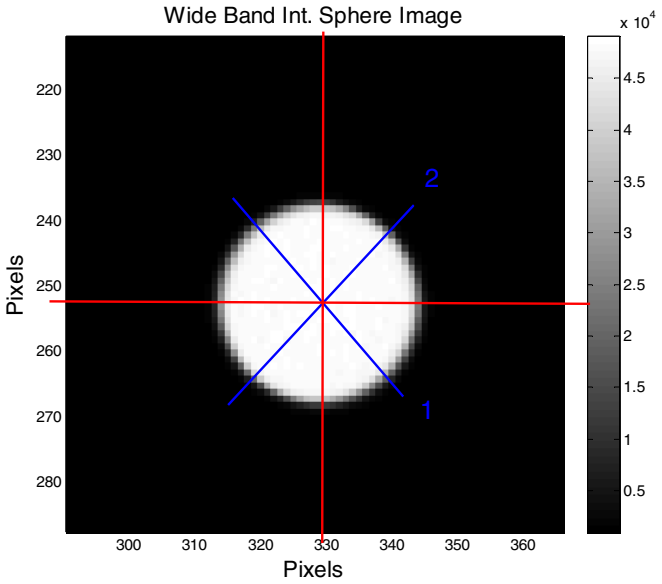

Figure 10. The four profiles extracted from the measurements.

(6027 for configuration B and 6029 for configuration A). Edge detection shows an almost perfect overlap of the images taken in the two configurations within a 2-pixel detection limit. Considering the area difference as the limit of a rectangular uncertainty distribution, the resulting standard uncertainty component due to residual blooming is 0.01%.

3.4. Lens distortions and chromatic aberration

It must be noted that our system, compared to the actual photographic cameras, has a limited resolution (0.26 megapixels) and that the custom-made lens has its focal point set to infinity. Hence, to evaluate lens distortions, such as barrel or pincushion ones, we considered the image of the exit port of the integrating sphere switched off (see figure 8). The image of the exit port circle can be considered a precision circle. We measured the length (in pixels) of four diameters oriented as shown in figure 10.

Horizontal and vertical lines have the same length while diagonal ones are 0.5 pixels longer. The corresponding standard uncertainty component, evaluated as the limit of a rectangular distribution, is estimated to be 0.05%.

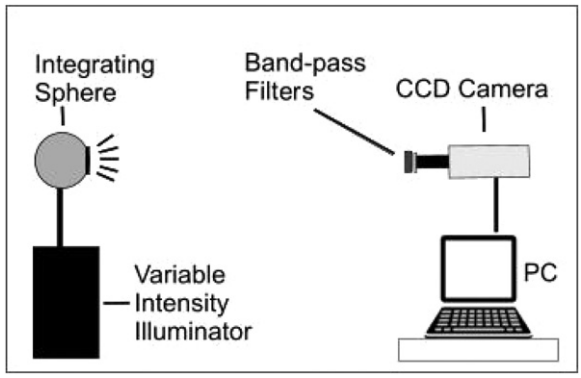

Figure 12. The experimental setup to evaluate residual chromatic aberration.

Chromatic aberration is a type of distortion in which there is a failure of a lens to focus all wavelengths to the same convergence point. It occurs because lenses have a different refractive index for different wavelengths (see figure 11) [15]. Chromatic aberration can be seen as a blurring effect that can be visually identified as an unfocused image; in practice it causes an 'enlargement' of the observed object and an error in pixel intensity readout [1]. Chromatic aberration can be minimized using an achromatic lens system, in which materials with different amounts of dispersion are assembled together to form a compound lens. The most common type is an achromatic doublet which reduces the amount of chromatic aberration over a defined range of wavelengths, although it does not produce a perfect correction.

To evaluate the residual chromatic aberration effect of the lens system, spectral measurements of an illuminated integrating sphere were performed. In detail, seven different spectral band-pass filters in the 400–450, 450–500, 500–600, 600–700, 700–800, 800–900 and 900–1100 nm spectral bands were considered (see figure 12).

Several images of the integrating sphere's exit port in the seven spectral bands plus the wide band (i.e. no band-pass filters) configurations have been acquired at a constant illumination level. As a result we obtained eight groups of measurements. For each group an average image was evaluated and from each averaged image four profiles (horizontal, vertical, diagonal1 and diagonal2) were defined as shown in figure 10. The extracted profiles were grouped according to their orientation and plotted on top of each other.

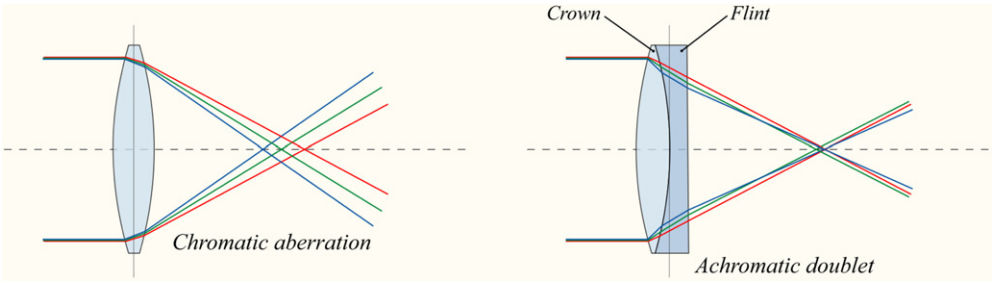

Figure 11. Chromatic aberration causes different wavelengths of light to have differing focal lengths. For an achromatic doublet, visible wavelengths have approximately the same focal length (adapted from [16]).

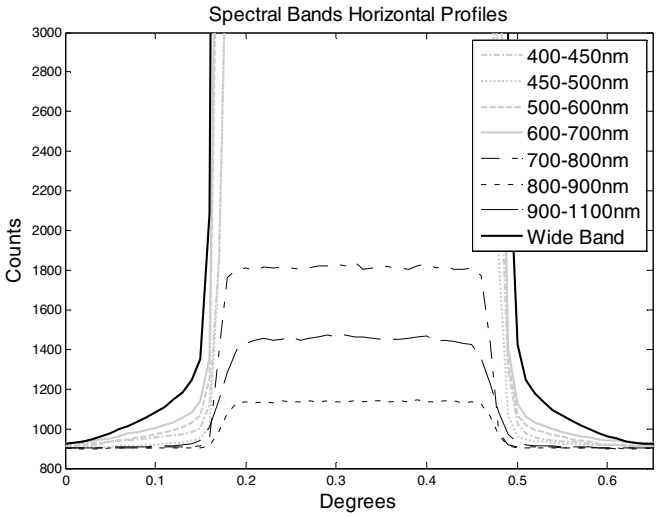

Figure 13. Details of the eight profiles in the horizontal orientation.

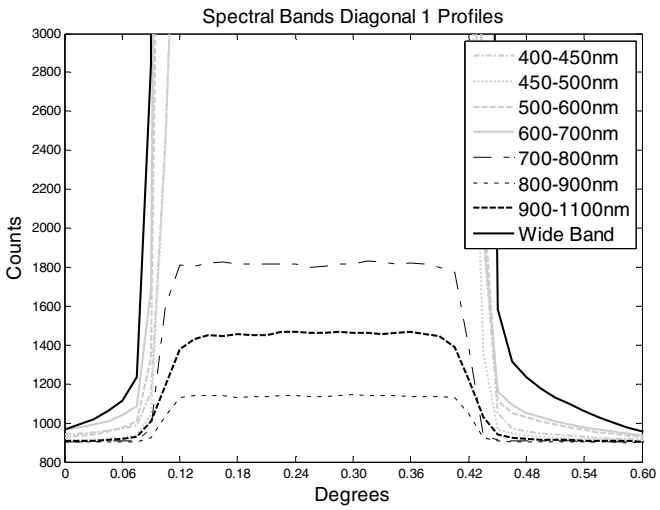

Figure 15. Details of the eight profiles in the diagonal1 orientation.

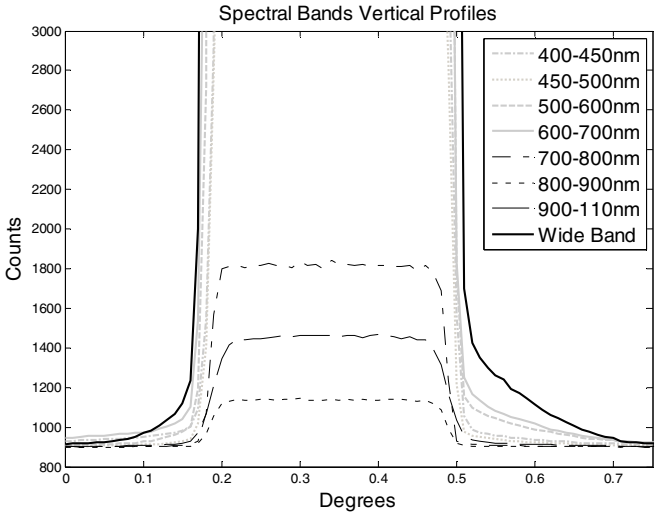

Figure 14. Details of the eight profiles in the vertical orientation.

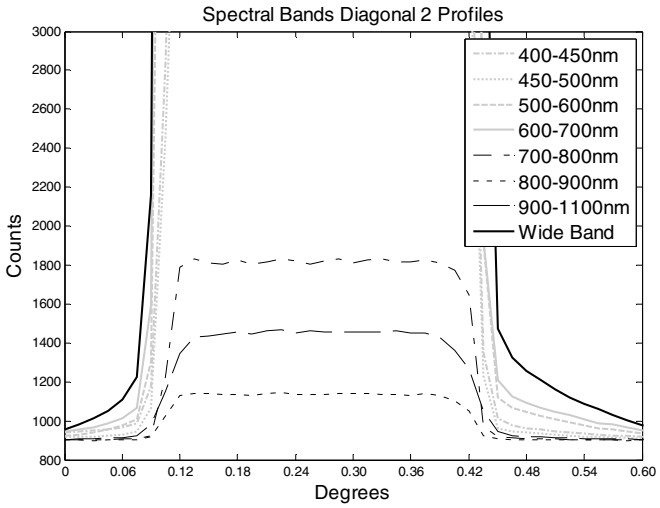

Figure 16. Details of the eight profiles in the diagonal2 orientation.

The graphical comparison of the eight profiles provides an estimation of the residual chromatic aberration.

To highlight the broadening effect, details of the eight profile graphs, for the four orientations, are shown in figures 13–16. The differences in the profiles are quantifiable in 3–4 pixels, i.e. less than 0.05°. In figures 14–16 a slight asymmetry between the left and the right sides of the profiles is also evident. Our hypothesis is that the asymmetry is given by the charge flow between the pixels that, due to the CCD architecture, has a preferential orientation along the columns and with a downward direction.

The standard uncertainty component due to the residual chromatic aberration effect was evaluated considering the 0.05° profile broadening as the limit of a rectangular distribution and estimated to be 0.28%.

Hence, the total standard uncertainty due to lens distortions and chromatic aberration is 0.29%.

3.5. Exposure time linearity

To evaluate the linearity of the system response to the variation of the exposure time an indoor experiment has been carried out. In detail, measurements of an integrating sphere were acquired at different exposure times (from 6 to 60 ms) keeping the integrating sphere output intensity constant. During the experiment the stability of the light source was evaluated to be within ±2.6%. In this case the pixel count values ranged from 55 900 counts for the highest exposure time (60 ms) down to 23 100 counts for the lowest exposure time (6 ms). The measurement results are shown in figure 17 together with the linear fitting. Figure 17 clearly shows a nonlinearity which is confirmed by the linearity test results (5.56%) and the correlation coefficient (0.8895).

Due to the large nonlinearity of results when changing the exposure time, we decided not to change it by more than 3% during the whole measurement campaign, keeping

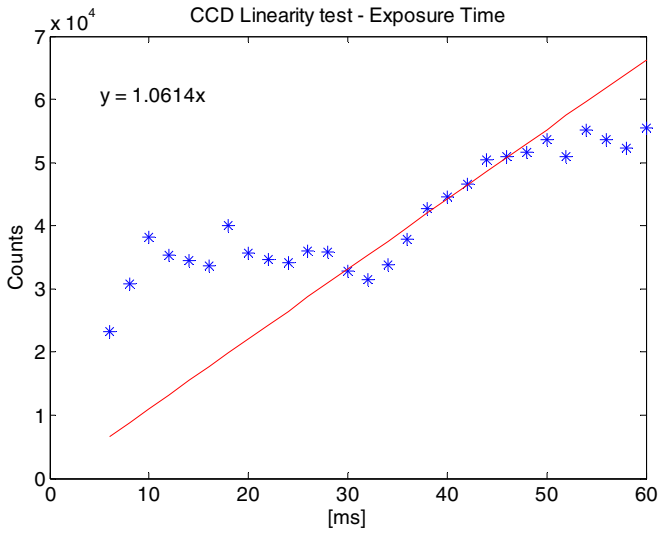

Figure 17. Analysis of the results of the exposure time linearity test.

Table 2. Measurement standard uncertainties relative to system dynamics.

Uncertainty source	Uncertainty %
Background noise	0.01
Linearity	0.35
Blooming	0.01
Lens distortions	0.29
CCD quantization error	0.12
Combined expanded uncertainty ($k = 2$)	0.94

this component negligible. Hence to ensure that the system is operating within its linearity range it is necessary to keep the exposure time fixed during a single measurement session.

3.6. Quantization and uncertainty budget

Since in our case the CCD-camera-based measurement system is used to measure the solar radial energy distribution falling at different solid angles, a further uncertainty source to be considered is the quantization error due to the finite CCD array spatial resolution, which has a rectangular distribution. Since the focus of the lens system is at infinity, pixel angular and spatial resolutions can be considered equal, considering that for the CCD-camera and lens system geometry this value is 0.011°. Hence, the standard uncertainty due to quantization error is equal to 0.12% ($k = 1$).

Finally, the combined expanded uncertainty relative to system dynamics is 0.94% ($k = 2$). A coverage factor $k = 2$, for a Gaussian probability distribution, defines an interval having a confidence level of approximately 95%. The evaluated uncertainty components and the combined expanded uncertainty are summarized in table 2.

4. Conclusions

A high resolution CCD-camera-based measurement system has been tested and characterized to evaluate the uncertainty of its response for solar radial energy distribution measurements. Several uncertainty sources were considered in evaluating an overall value for the measurement system, namely CCD linearity and background noise, blooming, lens and chromatic aberrations, exposure time linearity and quantization error. The working hypothesis was that, provided the measurement system is working within its linearity range, an absolute irradiance calibration is not needed and pyrheliometer data can be used to scale the measurement outputs into irradiance levels.

Experimental results showed that if the system measurements are kept below 56 000 counts, an expanded combined uncertainty equal to 0.94% ($k = 2$) relative to system dynamics can be assumed. It must be noted that in the actual system configuration the larger uncertainty contributions come from pixel linearity and residual chromatic aberration. The latter can be improved using an achromatic triplet lens.

Acknowledgments

The authors would like to gratefully acknowledge Ewan Dunlop, Thomas Huld, Nigel Taylor and Willem Zaaiman (ESTI) for their help and useful comments.

References

[1] Fiorentin P, Iacomussi P and Rossi G 2005 Characterization and calibration of a CCD detector for light engineering *IEEE Trans. Instrum. Meas.* **54** 171–7

[2] Simpson M L and Jansen J F 1991 Imaging colorimetry: a new approach *Appl. Opt.* **30** 4666–71

[3] Ferrero A, Campos J and Pons A 2006 Low-uncertainty absolute radiometric calibration of a CCD *Metrologia* **43** S17–21

[4] Ortiz A and Oliver G 2006 Radiometric calibration of vision cameras and intensity uncertainty estimation *Image Vis. Comput.* **24** 1137–45

[5] Neumann A and Schubnell M 1992 Irradiance and sunshape measurements for the Cologne site *Proc. 8th Int. Solar Forum* pp 1173–83

[6] Neumann A, von der Au B and Heller P 1998 Measurements of circumsolar radiation at the Plataforma Solar (Spain) and at DLR (Germany) *Proc. Int. Solar Energy Conf.* pp 429–38

[7] Healey G E and Kondepudy R 1994 Radiometric CCD camera calibration and noise estimation *IEEE Trans. Pattern Anal. Mach. Intell.* **16** 267–76

[8] Iqbal M 1983 *An Introduction to Solar Radiation* (New York: Academic)

[9] Rabl A and Bendt P 1982 Effect of circumsolar radiation on performance of focusing collectors *J. Sol. Energy Eng.* **104** 237–50

[10] Benitez P and Minano J C 2003 Concentrator optics for the next generation photovoltaics *Next Generation Photovoltaics: High Efficiency Through Full Spectrum Utilization* ed A Marti and A Luque (Bristol: Institute of Physics Publishing)

[11] Buie D and Monger A G 2004 The effect of circumsolar radiation on a solar concentrating system *Sol. Energy* **76** 181–5

[12] JCGM 2008 *Evaluation of Measurement Data—Guide to the Expression of Uncertainty in Measurement* JCGM 100:2008 (GUM 1995 with minor corrections) Available at http://www.iso. org/sites/JCGM/GUM-introduction.htm

[13] ASTM 2010 International Standard test method for determining the linearity of a photovoltaic device parameter with respect to a test parameter *Designation* E1143-05 pp 592–3

[14] Haapalinna A, Kubarsepp T, Karha P and Ikonen E 1999 Measurement of the absolute linearity of photodetectors with a diode laser *Meas. Sci. Technol.* **10** 1075–8

[15] Born M and Wolf E 1999 *Principles of Optics* 7th edn (Cambridge: Cambridge University Press)

[16] Wikipedia http://en.wikipedia.org/wiki/Chromatic_aberration (20 February 2011)